

Tricritical wings and modulated magnetic phases in LaCrGe_3 under pressure

Udhara S. Kaluarachchi,^{1,2} Sergey L. Bud'ko,^{1,2} Paul C. Canfield,^{1,2} and Valentin Taufour^{a1}

¹*The Ames Laboratory, US Department of Energy,
Iowa State University, Ames, Iowa 50011, USA*

²*Department of Physics and Astronomy,
Iowa State University, Ames, Iowa 50011, U.S.A.*

Abstract

We determined on the temperature-pressure-magnetic field (T - p - H) phase diagram of the ferromagnet LaCrGe_3 from electrical resistivity measurements on single crystals. In ferromagnetic systems, quantum criticality is avoided either by a change of the transition order, becoming of the first order at a tricritical point, or by the appearance of modulated magnetic phases. In the first case, the application of a magnetic field reveals a wing-structure phase diagram as seen in itinerant ferromagnets such as ZrZn_2 and UGe_2 . In the second case, no tricritical wings have been observed so far. Our investigation of LaCrGe_3 reveals a double-wing structure indicating strong similarities with ZrZn_2 and UGe_2 . But, unlike these, simpler systems, LaCrGe_3 is thought to exhibit a modulated magnetic phase under pressure which already precludes it from a pressure-driven paramagnetic-ferromagnetic quantum phase transition in zero field. As a result, the T - p - H phase diagram of LaCrGe_3 shows both the wing structure as well as the appearance of new magnetic phases, providing the first example of this new possibility for the phase diagram of metallic quantum ferromagnets.

^a Present address University of California, Davis

Suppressing a second-order, magnetic phase transition to zero temperature with a tuning parameter (pressure, chemical substitutions, magnetic field) has been a very fruitful way to discover many fascinating phenomena in condensed matter physics. In the region near the putative quantum critical point (QCP), superconductivity has been observed in antiferromagnetic [1] as well as ferromagnetic systems [2–4]. One peculiarity of the clean ferromagnetic systems studied so far is that the nature of the paramagnetic-ferromagnetic (PM-FM) phase transition always changes before being suppressed to zero temperature [5]: in most cases, the transition becomes of the first order [6–11]. Recently, another possibility, where a modulated magnetic phase (AFM_Q) appears (spin-density wave, antiferromagnetic order), has been observed in CeRuPO [12, 13], MnP [14, 15] and LaCrGe₃ [16]. When a FM transition becomes of the first order at a tricritical point (TCP) in the temperature T pressure p plane, the application of a magnetic field H along the magnetization axis reveals a wing structure phase diagram in the T - p - H space. This is seen in UGe₂ [17, 18] and ZrZn₂ [19] and is schematically represented in Fig.1a. This phase diagram shows the possibility of a new kind of quantum criticality at the quantum wing critical point (QWCP). In contrast with the conventional QCP, symmetry is already broken by the magnetic field at a QWCP. In the more recently considered case where the transition changes to a AFM_Q phase, no wing structure phase diagram has been reported, but it is found that the AFM_Q is suppressed by moderate magnetic field [12, 13]. This second possible T - p - H phase diagram has been schematically presented in a recent review [5] and reproduced in Fig.1b.

Here, we report electrical resistivity measurements on LaCrGe₃ under pressure and magnetic field. We determine the T - p - H phase diagram and find that it corresponds to a third possibility where tricritical wings emerge in addition to the AFM_Q phase. This new type of phase diagram is illustrated in Fig.1c: it includes both the tricritical wings and the AFM_Q phase. In addition, the phase diagram of LaCrGe₃ shows a double wing structure similar to what is observed in the itinerant ferromagnets UGe₂ [20] and ZrZn₂ [21], but with the additional AFM_Q phase. LaCrGe₃ is the first example showing such a phase diagram.

Recently, we reported on the T - p phase diagram of LaCrGe₃ [16], which is reproduced in Fig.1d. At ambient pressure, LaCrGe₃ orders ferromagnetically at $T_C = 86$ K. Under applied pressure, T_C decreases and disappears at 2.1 GPa. Near 1.3 GPa, there is a Lifshitz point at which a new transition line appears. The new transition corresponds to the appearance of a modulated magnetic phase (AFM_Q) and can be tracked up to 5.2 GPa. Muon-spin rotation

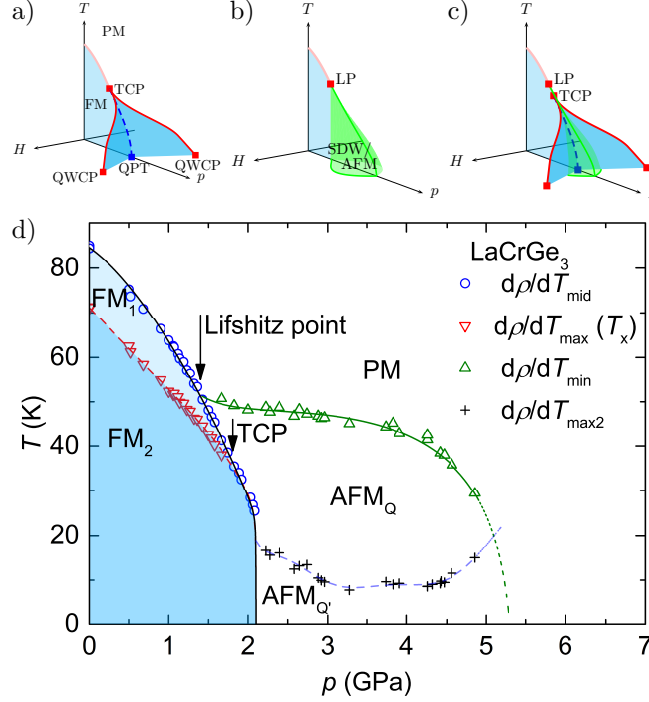


FIG. 1. (Color online) a) Schematic T - p - H phase diagram of a quantum ferromagnet: the paramagnetic-ferromagnetic (PM-FM) transition becomes of the first order at a tricritical point (TCP) after which there is a quantum phase transition (QPT) at 0 K. Tricritical wings emerge from the TCP under magnetic field and terminate at quantum wing critical points (QWCP). b) Schematic T - p - H phase diagram of a quantum ferromagnet when a modulated magnetic phase (SDW/AFM) emerges from the Lifshitz point (LP). c) New possible schematic T - p - H phase diagram for which tricritical wings as well as a new magnetic phase are observed. d) T - p phase diagram of LaCrGe_3 from electrical resistivity measurements [16] showing two FM regions (FM_1 and FM_2) separated by a crossover.

(μSR) measurements show that the AFM_Q phase has a similar magnetic moment as the FM phase but without net macroscopic magnetization [16]. In addition, band structure calculations suggest that the AFM_Q phase is characterized by a small wave-vector Q and that several small Q phases are nearly degenerate. Below the PM- AFM_Q transition line, several anomalies marked as gray cross in Fig.1d can be detected in $\rho(T)$ [16]. These other anomalies within the AFM_Q phase are compatible with the near degeneracy of different Q -states (shown as AFM_Q and $\text{AFM}_{Q'}$) with temperature and pressure driven transitions between states with differing wavevectors.

RESULTS

In this article, we determine the three dimensional T - p - H phase diagram of LaCrGe_3 by measuring the electrical resistivity of single crystals of LaCrGe_3 under pressure and magnetic field. The sample growth and characterization has been reported in Ref. [22]. The pressure techniques have been reported in Ref. [16]. The magnetic field dependent resistivity was measured in two Quantum Design Physical Property Measurement Systems up to 9 or 14 T. The electrical current is in the ab -plane, and the field is applied along the c -axis, which is the easy axis of magnetization [22, 23].

Whereas most of the features in Fig.1d were well understood in Ref. [16], we also indicate the pressure dependence of T_x ($d\rho/dT_{\text{max}}$) at which a broad maximum is observed in $d\rho/dT$ below T_C and shown as orange triangles in Fig.1d. At ambient pressure, $T_x \approx 71$ K. No corresponding anomaly can be observed in magnetization [16], internal field [16] or specific heat [22]. Under applied pressure, T_x decreases and cannot be distinguished from T_C ($d\rho/dT_{\text{mid}}$) above 1.6 GPa. As will be shown, application of magnetic field allows for a much clearer appreciation and understanding of this feature.

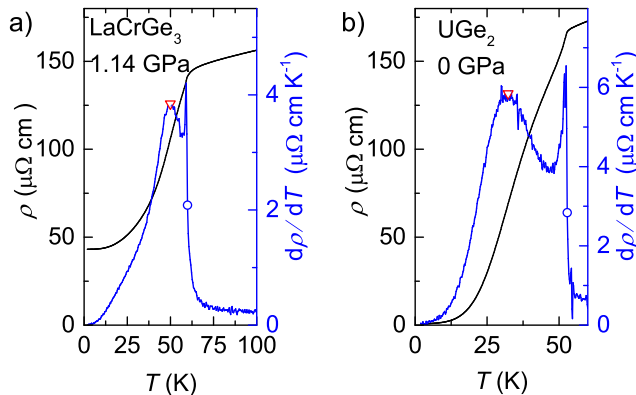


FIG. 2. (color online) Temperature dependence of the resistivity (black line) and its derivative (blue line) of (a) LaCrGe_3 at 1.14 GPa and (b) UGe_2 at 0 GPa from Ref. [17]. The crossover between the two ferromagnetic phases (FM1 and FM2) is inferred from the maximum in $d\rho/dT$ (T_x) and marked by a red triangle, whereas the paramagnetic-ferromagnetic transition is inferred from the middle point of the sharp increase in $d\rho/dT$ (T_C) and indicated by a blue circle.

Figure 2a shows the anomalies at T_x and T_C observed in the electrical resistivity and its

temperature derivative at 1.14 GPa. For comparison, Fig. 2b shows ambient pressure data for UGe_2 [17] where a similar anomaly at T_x can be observed. In UGe_2 , this anomaly was studied intensively [24–26]. It corresponds to a crossover between two ferromagnetic phases FM1 and FM2 with different values of the saturated magnetic moment [24, 25]. Under pressure, there is a critical point at which the crossover becomes a first-order transition, which eventually vanishes where a maximum in superconducting-transition temperature is observed [2]. In the case of LaCrGe_3 , we cannot locate where the crossover becomes a first order transition, since the anomaly merges with the Curie temperature anomaly near 1.6 GPa, very close to the TCP. However, as we will show below, the two transitions can be separated again with applied magnetic field above 2.1 GPa. This is similar to what is observed in UGe_2 where the PM-FM1 and FM1-FM2 transition lines separate more and more as the pressure and the magnetic field are increased. Because of such similarities with UGe_2 , we label the two phases FM1 and FM2 and assume that the anomaly at T_x corresponds to a FM1-FM2 crossover. A similar crossover was also observed in ZrZn_2 [21]. In Refs. [27, 28], a Stoner model with two peaks in the density of states near the Fermi level was proposed to account for the two phases FM1 and FM2, reinforcing the idea of the itinerant nature of the magnetism in LaCrGe_3 .

In zero field, for applied pressures above 2.1 GPa, both FM1 and FM2 phases are suppressed. Upon applying a magnetic field along the c -axis, two sharp drops of the electrical resistivity can be observed (Fig.3a) with two corresponding minima in the field derivatives (Fig.3b). At 2 K, clear hysteresis of $\Delta H \sim 0.7$ T can be observed for both anomalies indicating the first order nature of the transitions. The emergence of field-induced first-order transitions starting from 2.1 GPa and moving to higher field as the pressure is increased is characteristic of the ferromagnetic quantum phase transition: when the PM-FM transition becomes of the first order, a magnetic field applied along the magnetization axis can induce the transition resulting in a wing structure phase diagram such as the one illustrated in Fig.1a. In the case of LaCrGe_3 , evidence for a first order transition was already pointed out because of the very steep pressure dependence of T_C near 2.1 GPa and the abrupt doubling of the residual ($T = 2$ K) electrical resistivity [16]. In UGe_2 or ZrZn_2 , the successive metamagnetic transitions correspond to the PM-FM1 and FM1-FM2 transitions. In LaCrGe_3 , due to the presence of the AFM_Q phase at zero field, the transitions correspond to AFM_Q -FM1 and FM1-FM2.

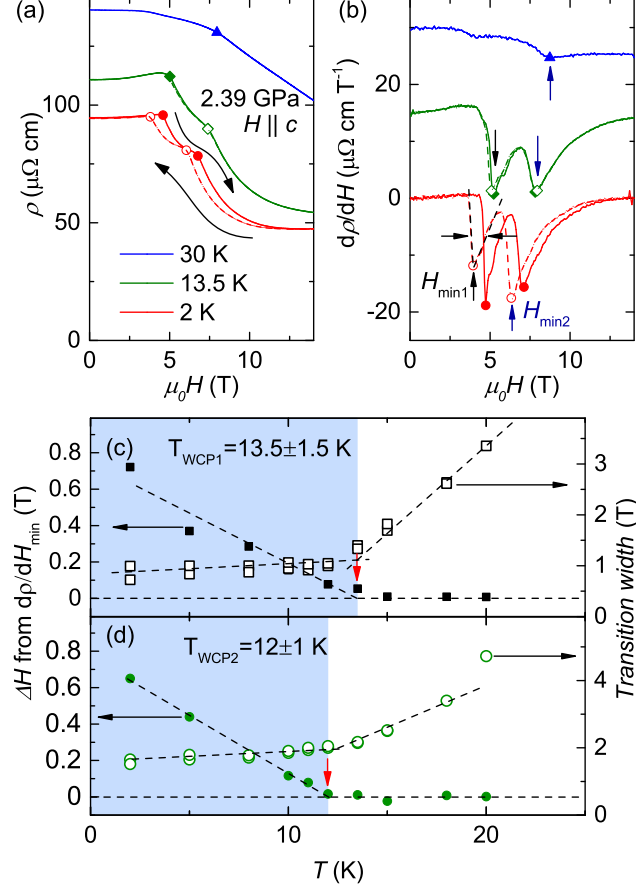


FIG. 3. (color online) (a) Field dependence of the electrical resistivity at 2 K, 13.5 K, and 30 K at 2.39 GPa. Continuous and dashed lines represent the field increasing and decreasing respectively. (b) Corresponding field derivatives ($d\rho/dH$). The curves are shifted by $15 \mu\Omega \text{ cm T}^{-1}$ for clarity. Vertical arrows represent the minima. The transition width is determined by the full width at half minimum as represented by horizontal arrows. The temperature dependence of the hysteresis width of H_{min1} and H_{min2} are shown in (c) and (d)(left axes). The hysteresis width gradually decreases with increasing temperature and disappears at T_{WCP} . The right axes show the temperature dependence of the transition widths. The width is small for the first-order transition and becomes broad in the crossover region. The blue-color shaded area represents the first order transition region whereas the white color area represents the crossover region. These allow for the determination of the wing critical point of the FM1 transition at 13.5 K, 2.39 GPa and 5.1 T and the one for the FM2 transition at 12 K, 2.39 GPa and 7.7 T.

As the temperature is increased, the hysteresis decreases for both transitions, as can be

seen in Figs. 3c and d and disappears at a wing critical point (WCP). Also, the transition width is small and weakly temperature dependent below the WCP and it broadens when entering in the crossover regime. Similar behavior has been observed in UGe_2 [18]. At 2.39 GPa for example, we locate the WCP of the first-order FM1 transition around 13.5 K and the one of the first-order FM2 transition around 12 K. At this temperature and pressure, the transitions occur at 5.1 and 7.7 T respectively. This allows for the tracking of the wing boundaries in the T - p - H space up to our field limit of 14 T. At low field, near the TCP, the wing boundaries are more conveniently determined as the location of the largest peak in $d\rho/dT$ (Supplementary Information).

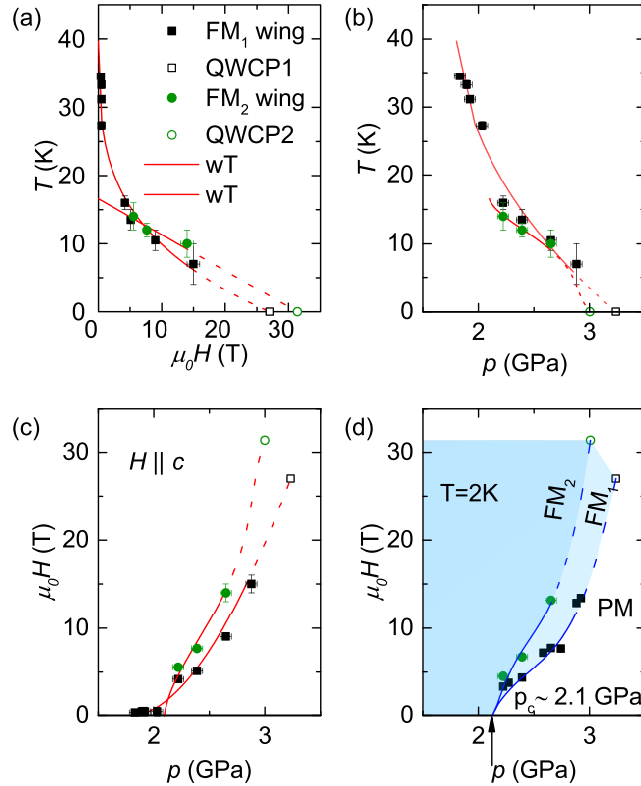


FIG. 4. (color online) Projection of the wings in (a) T - H , (b) T - p and (c) H - p planes. Black solid squares and green solid circles represents the FM₁-wing and FM₂-wing respectively. Red lines (represented in the T - p - H space in Fig.5) are guides to the eyes and open symbols represent the extrapolated QWCP. (d) H - p phase diagram at 2K. The arrow represents the pressure $p_c = 2.1$ GPa.

The projections of the wings lines $T_{\text{WCP}}(p, H)$ in the T - H , T - p and H - p planes are shown

in Figs. 4a, b and c respectively. The metamagnetic transitions to FM1 and FM2 start from 2.1 GPa and separate in the high field region as the pressure is further increased. For the FM1 wing, the slope dT_w/dH_w is very steep near $H = 0$ (Fig. 4a) whereas dH_w/dp_w is very small (Fig. 4c). This is in agreement with a recent theoretical analysis based on the Landau expansion of the free energy which shows that dT_w/dH_w and dp_w/dH_w are infinite at the tricritical point [29]. This fact was overlooked in the previous experimental determinations of the wing structure phase diagram in UGe_2 [17, 18] and ZrZn_2 [19], but appears very clearly in the case of LaCrGe_3 . In the low field region, there are no data for the FM2 wing since the transition is not well separated from the FM1 wing, but there is no evidence for an infinite slope near $H = 0$. The wing lines can be extrapolated to quantum wing critical points (QWCPs) at 0 K in high magnetic fields of the order of ~ 30 T (Fig. 4a) and pressures around ~ 3 GPa (Fig. 4b). Figure 4d shows the p - H phase diagram at low temperature ($T = 2$ K). Identical H - p phase diagram in Fig. 4b and Fig. 4c reveals the near vertical nature of the wings.

The resulting three-dimensional T - p - H phase diagram of LaCrGe_3 is shown in Fig. 5 which summarizes our results (Several of the constituent T - H phase diagrams, at various pressures, are given in Supplementary Information). The double wing structure is observed in addition to the AFM_Q phase. This is the first time that such a phase diagram is reported. Other materials suggested that there is either a wing structure without any new magnetic phase [17–19], or a new magnetic phase without wing structure [12, 13]. The present study illustrates a third possibility where all such features are observed. Moreover, the existence of the two metamagnetic transitions (to FM1 and FM2) suggests that this might be a generic feature of itinerant ferromagnetism. Indeed, it is observed in ZrZn_2 , UGe_2 , and LaCrGe_3 , although these are very different materials with different electronic orbitals giving rise to the magnetic states. We note that a wing structure has also been determined in the paramagnetic compounds UCoAl [30–32] and $\text{Sr}_3\text{Ru}_2\text{O}_7$ [33], implying that a ferromagnetic state probably exists at negative pressures in these materials. Strikingly, two anomalies could be detected upon crossing the wings in UCoAl (two kinks of a plateau in electrical resistivity [30], two peaks in the ac susceptibility [32]), as well as in $\text{Sr}_3\text{Ru}_2\text{O}_7$ (two peaks in the ac susceptibility [33]). These double features could also correspond to a double wing structure.

To conclude, the T - p - H phase diagram of LaCrGe_3 provides an example of a new possible

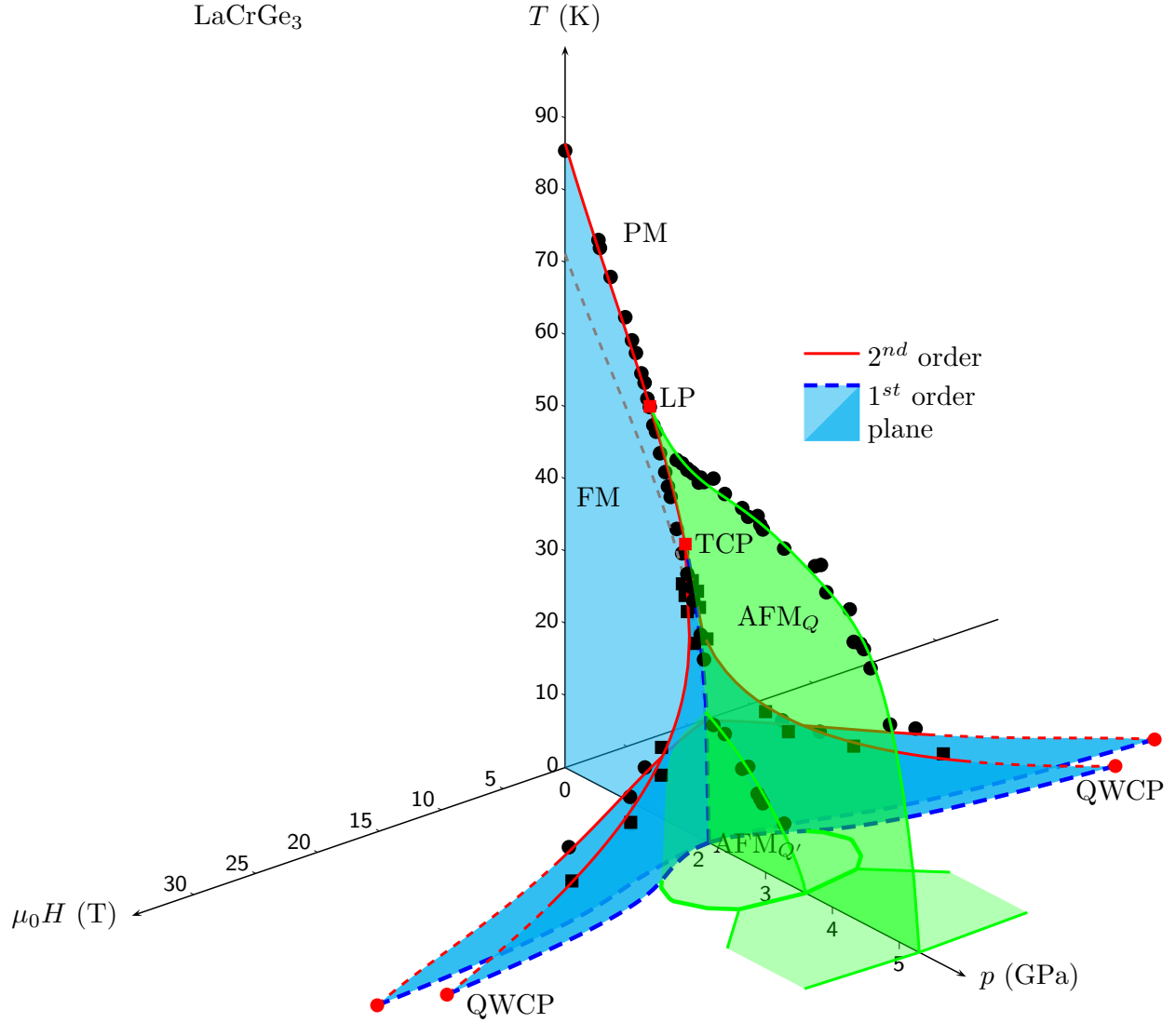


FIG. 5. (color online) T - p - H phase diagram of LaCrGe₃ based on resistivity measurements. Red solid lines are the second order phase transition and blue color planes are planes of first order transitions. Green color areas represent the AFM_Q phase.

outcome of ferromagnetic quantum criticality. At zero field, quantum criticality is avoided by the appearance of a new modulated magnetic phase, but the application of magnetic field shows the existence of a wing structure phase diagram leading towards QWCP at high field. These experimental findings reveal new insights into the possible phase-diagram of ferromagnetic systems. The emergence of the wings reveals for the first time a theoretically predicted tangent slope [29] near the tricritical point, a fact that was overlooked in previous experimental determination of phase diagrams of other compounds because of the lack of

data density in that region. In addition, the double nature of the wings appears to be a generic feature of itinerant ferromagnetism, as it is observed in several, a priori, unrelated materials. This result deserves further theoretical investigations and unification.

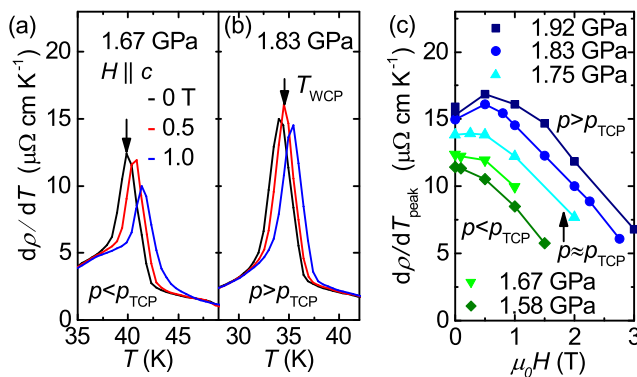
Acknowledgements We would like to thank S. K. Kim, X. Lin, V. G. Kogan, D. K. Finnemore, E. D. Mun, H. Kim, Y. Furukawa, R. Khasanov for useful discussions. This work was carried out at the Iowa State University and the Ames Laboratory, US DOE, under Contract No. DE-AC02-07CH11358. This work was supported by the Materials Sciences Division of the Office of Basic Energy Sciences of the U.S. Department of Energy.

Supplementary Information is attached below.

Author Contributions V. T. and P. C. initiated this study. U. K. and P. C. prepared the single crystals. U. K, V. T. and S. B. performed the pressure measurements. U. K, V. T, S. B. and U. K analysed and interpreted the pressure data. U. K. and V. T. wrote the manuscript with the help of all authors.

SUPPLEMENTARY INFORMATION

Determination of the location of the tricritical point



Supplementary Figure 6. (color online) (a)-(b) Temperature dependence of $d\rho/dT$ at various magnetic fields at 1.67 and 1.83 GPa. Arrow in panel (a) represent the T_C and panel (b) represent the T_{WCP} . (c) The variation of $d\rho/dT_{\text{peak}}$ as a function of external field for $p < p_{\text{TCP}}$, $p \approx p_{\text{TCP}}$ and $p_{\text{TCP}} < p < p_c$.

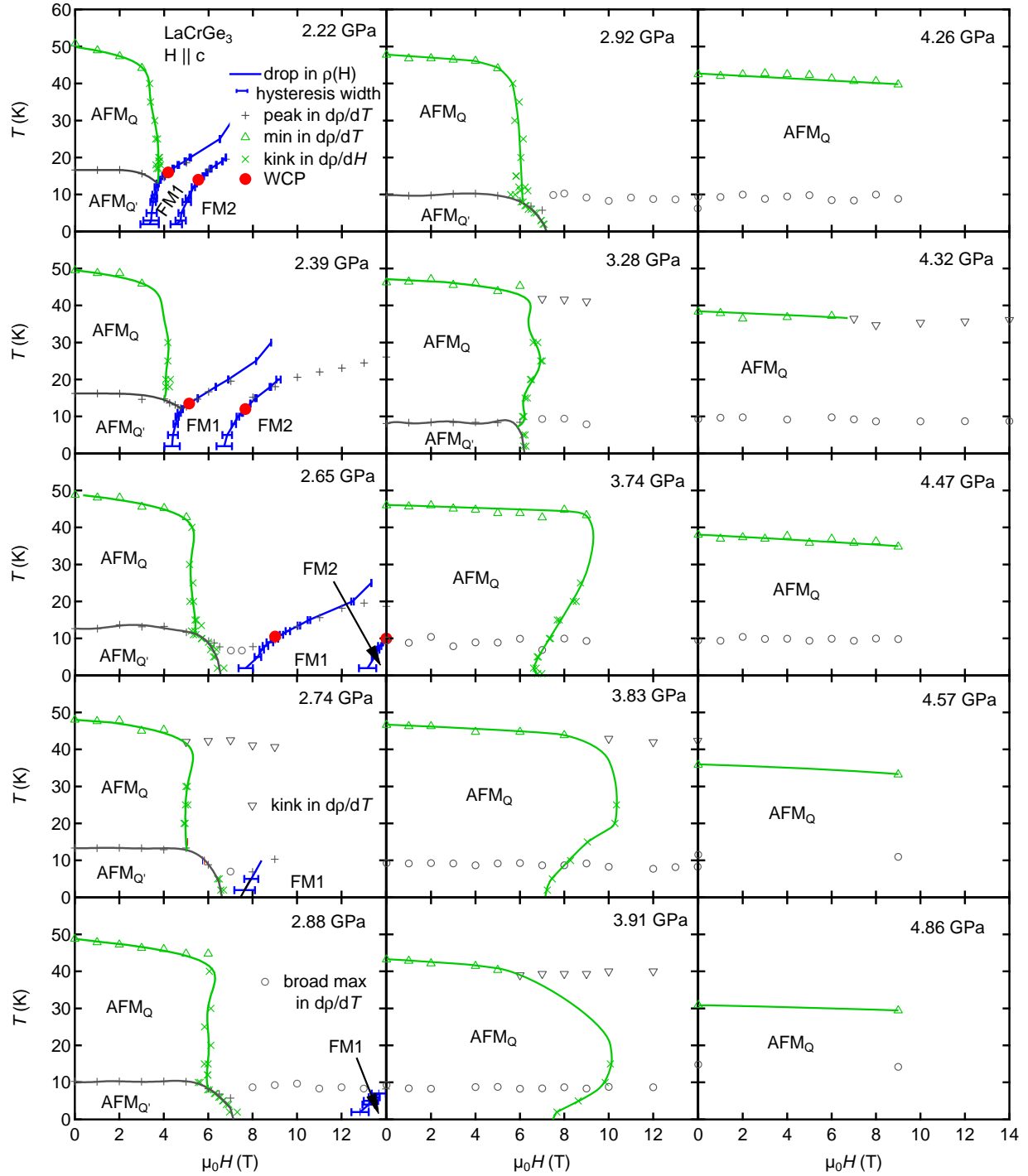
In Ref. [16], the position of the tricritical point TCP was estimated near 40 K and 1.75 GPa based on a discontinuity in the resistivity as a function of pressure $\rho(p)$. Here, we use measurements under magnetic field to locate the TCP. When the paramagnetic-ferromagnetic (PM-FM) transition is of the second order, the magnetic field applied along the magnetization axis (c -axis) breaks the time reversal symmetry, so that no phase transition can occur. Instead, a crossover is observed resulting in a broadening and disappearing of the anomalies. Supplementary Fig. 6a, shows the peak in the temperature derivative of resistivity $d\rho/dT$ at various magnetic fields at 1.67 GPa. The peak amplitude decreases showing that the transition is of the second order. This is in contrast with the behavior at 1.83 GPa (Supplementary Fig. 6b) where the peak first increases under magnetic field indicating the first order nature of the transition. The evolution of the value of $d\rho/dT$ at the peak position as a function of magnetic field is shown in Supplementary Fig. 6c for various pressures. We can distinguish two regimes: for pressures below ~ 1.75 GPa, the peak size monotonically decreases with applied magnetic field; for pressure above 1.75 GPa, the peak size first increases with field, reach a maximum at a field H_{WCP} and then decreases. With this procedure, we find the TCP to be near 1.75 GPa, at which pressure the transition temperature is 40 K.

For $p > p_{TCP}$, the location of the maximum value of $d\rho/dT$ at the peak position serves to locate the wing critical point as a function of temperature, pressure and magnetic field.

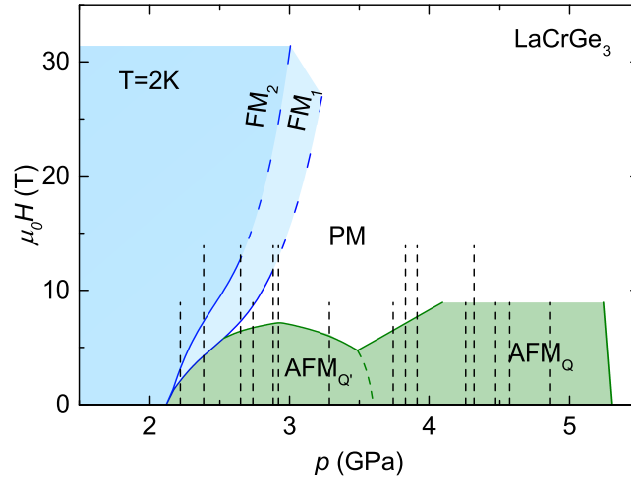
Determination of the three-dimensional T - p - H phase diagram

In Supplementary Fig.7, we show several T - H phase diagrams at various pressures (as illustrated in Supplementary Fig 8) . For each pressure, anomalies in the temperature and field dependence of the electrical resistivity are located and serve to outline the phase boundaries. To be complete, and for future reference, we also indicate the location of broad maxima or kinks in $d\rho/dT$ which do not seem to correspond to phase transitions at this point and are most likely related to crossover anomalies.

The T - p - H phase diagram shown as Fig.5 in the main text is constructed by combining all the T - H phase diagrams at various pressures.



Supplementary Figure 7. (color online) Compilation of T - H phase diagrams at various pressures determined by tracking various anomalies in the temperature and field dependence of the electrical resistivity measurements up to 9 or 14 T. The hysteresis width for the drop in $\rho(H)$ (minimum in $d\rho/dH$) is also indicated. Lines are guides to the eyes. The pressure positions are shown in Supplementary Fig. 8.



Supplementary Figure 8. p - H phase diagram of LaCrGe₃ at 2 K. the black dashed lines indicate the position of the pressures for the diagrams shown in Supplementary Fig. 7. Note: This is an expanded view of diagram shown in Figs. 4d in main text

-
- [1] N. Mathur, F. Grosche, S. Julian, I. Walker, D. Freye, R. Haselwimmer, and G. Lonzarich, *Nature* **394**, 39 (1998).
- [2] S. S. Saxena *et al.*, *Nature (London)* **406**, 587 (2000).
- [3] D. Aoki, A. D. Huxley, E. Ressouche, D. Braithwaite, J. Flouquet, J. Brison, E. Lhotel, and C. Paulsen, *Nature (London)* **413**, 613 (2001).
- [4] N. T. Huy, A. Gasparini, D. E. de Nijs, Y. Huang, J. C. P. Klaasse, T. Gortenmulder, A. de Visser, A. Hamann, T. Gorlach, and H. v. Lohneysen, *Phys. Rev. Lett.* **99**, 067006 (2007).
- [5] M. Brando, D. Belitz, F. M. Grosche, and T. R. Kirkpatrick, *Rev. Mod. Phys.* **88**, 025006 (2016).
- [6] T. Goto, Y. Shindo, H. Takahashi, and S. Ogawa, *Phys. Rev. B* **56**, 14019 (1997).
- [7] A. D. Huxley, I. Sheikin, and D. Braithwaite, *Physica B* **284**, 1277 (2000).
- [8] M. Uhlarz, C. Pfleiderer, and S. M. Hayden, *Phys. Rev. Lett.* **93**, 256404 (2004).
- [9] E. Colombier, D. Braithwaite, G. Lapertot, B. Salce, and G. Knebel, *Phys. Rev. B* **79**, 245113 (2009).
- [10] S. Araki, M. Hayashida, N. Nishiumi, H. Manabe, Y. Ikeda, T. C. Kobayashi, K. Murata, Y. Inada, P. Wisniewski, D. Aoki, Y. Onuki, E. Yamamoto, and Y. Haga, *J. Phys. Soc. Jpn.* **84**, 024705 (2015).
- [11] Y. Shimizu, D. Braithwaite, B. Salce, T. Combier, D. Aoki, E. N. Hering, S. M. Ramos, and J. Flouquet, *Phys. Rev. B* **91**, 125115 (2015).
- [12] H. Kotegawa, T. Toyama, S. Kitagawa, H. Tou, R. Yamauchi, E. Matsuoka, and H. Sugawara, *J. Phys. Soc. Jpn.* **82**, 123711 (2013).
- [13] E. Lengyel, M. E. Macovei, A. Jesche, C. Krellner, C. Geibel, and M. Nicklas, *Phys. Rev. B* **91**, 035130 (2015).
- [14] J.-G. Cheng, K. Matsubayashi, W. Wu, J. P. Sun, F. K. Lin, J. L. Luo, and Y. Uwatoko, *Phys. Rev. Lett.* **114**, 117001 (2015).
- [15] M. Matsuda, F. Ye, S. E. Dissanayake, J.-G. Cheng, S. Chi, J. Ma, H. D. Zhou, J.-Q. Yan, S. Kasamatsu, O. Sugino, T. Kato, K. Matsubayashi, T. Okada, and Y. Uwatoko, *Phys. Rev. B* **93**, 100405 (2016).

- [16] V. Taufour, U. S. Kaluarachchi, R. Khasanov, M. C. Nguyen, Z. Guguchia, P. K. Biswas, P. Bonfà, R. De Renzi, X. Lin, S. K. Kim, E. D. Mun, H. Kim, Y. Furukawa, C.-Z. Wang, K.-M. Ho, S. L. Bud'ko, and P. C. Canfield, *Phys. Rev. Lett.* **117**, 037207 (2016).
- [17] V. Taufour, D. Aoki, G. Knebel, and J. Flouquet, *Phys. Rev. Lett.* **105**, 217201 (2010).
- [18] H. Kotegawa, V. Taufour, D. Aoki, G. Knebel, and J. Flouquet, *J. Phys. Soc. Jpn.* **80**, 083703 (2011).
- [19] N. Kabeya, H. Maekawa, K. Deguchi, N. Kimura, H. Aoki, and N. K. Sato, *J. Phys. Soc. Jpn.* **81**, 073706 (2012).
- [20] V. Taufour, A. Villaume, D. Aoki, G. Knebel, and J. Flouquet, in *Journal of Physics: Conference Series*, Vol. 273 (IOP Publishing Ltd., UK, 2011) p. 012017, International Conference on Strongly Correlated Electron Systems (SCES 2010), Santa Fe, NM, USA.
- [21] N. Kimura, M. Endo, T. Isshiki, S. Minagawa, A. Ochiai, H. Aoki, T. Terashima, S. Uji, T. Matsumoto, and G. G. Lonzarich, *Phys. Rev. Lett.* **92**, 197002 (2004).
- [22] X. Lin, V. Taufour, S. L. Bud'ko, and P. C. Canfield, *Phys. Rev. B* **88**, 094405 (2013).
- [23] J. M. Cadogan, P. Lemoine, B. R. Slater, A. Mar, and M. Avdeev, *Solid State Phenom.* **194**, 71 (2013).
- [24] C. Pfleiderer and A. D. Huxley, *Phys. Rev. Lett.* **89**, 147005 (2002).
- [25] F. Hardy, C. Meingast, V. Taufour, J. Flouquet, H. v. Loehneysen, R. A. Fisher, N. E. Phillips, A. D. Huxley, and J. C. Lashley, *Phys. Rev. B* **80**, 174521 (2009).
- [26] A. Palacio Morales, A. Pourret, G. Knebel, G. Bastien, V. Taufour, D. Aoki, H. Yamagami, and J. Flouquet, *Phys. Rev. B* **93**, 155120 (2016).
- [27] K. G. Sandeman, G. G. Lonzarich, and A. J. Schofield, *Phys. Rev. Lett.* **90**, 167005 (2003).
- [28] M. M. Wysokinski, M. Abram, and J. Spalek, *Phys. Rev. B* **90**, 081114 (2014).
- [29] V. Taufour, U. S. Kaluarachchi, and V. G. Kogan, *Phys. Rev. B* **94**, 060410 (2016).
- [30] D. Aoki, T. Combier, V. Taufour, T. D. Matsuda, G. Knebel, H. Kotegawa, and J. Flouquet, *J. Phys. Soc. Jpn.* **80**, 094711 (2011).
- [31] T. Combier, D. Aoki, G. Knebel, and J. Flouquet, *J. Phys. Soc. Jpn.* **82**, 104705 (2013).
- [32] N. Kimura, N. Kabeya, H. Aoki, K. Ohyama, M. Maeda, H. Fujii, M. Kogure, T. Asai, T. Komatsubara, T. Yamamura, and I. Satoh, *Phys. Rev. B* **92**, 035106 (2015).
- [33] W. Wu, A. McCollam, S. A. Grigera, R. S. Perry, A. P. Mackenzie, and S. R. Julian, *Phys. Rev. B* **83**, 045106 (2011).

